

KEK-preprint-94-177  
 DPNU-94-58  
 NWU-HEP 94-08  
 TIT-HPE-94-13  
 TUAT-HEP 94-08  
 OCU-HEP 94-10  
 PU-94-691  
 INS-REP 1076  
 KOBE-HEP 94-09

# Observation of Excess $\Lambda(\bar{\Lambda})$ Production in Two-Photon Processes at TRISTAN \*

(TOPAZ Collaboration)

R.Enomoto<sup>a†</sup>, K.Abe<sup>b</sup>, T.Abe<sup>b</sup>, I.Adachi<sup>a</sup>, K.Adachi<sup>c</sup>, M.Aoki<sup>d</sup>, M.Aoki<sup>b</sup>, S.Awa<sup>c</sup>, K.Emi<sup>e</sup>, H.Fujii<sup>a</sup>, K.Fujii<sup>a</sup>, T.Fujii<sup>f</sup>, J.Fujimoto<sup>a</sup>, K.Fujita<sup>g</sup>, N.Fujiwara<sup>c</sup>, H.Hayashii<sup>c</sup>, B.Howell<sup>h</sup>, N.Iida<sup>a</sup>, R.Itoh<sup>a</sup>, Y.Inoue<sup>g</sup>, H.Iwasaki<sup>a</sup>, M.Iwasaki<sup>c</sup>, K.Kaneyuki<sup>d</sup>, R.Kajikawa<sup>b</sup>, S.Kato<sup>i</sup>, S.Kawabata<sup>a</sup>, H.Kichimi<sup>a</sup>, M.Kobayashi<sup>a</sup>, D.Koltick<sup>h</sup>, I.Levine<sup>h</sup>, S.Minami<sup>d</sup>, K.Miyabayashi<sup>b</sup>, A.Miyamoto<sup>a</sup>, K.Muramatsu<sup>c</sup>, K.Nagai<sup>j</sup>, K.Nakabayashi<sup>b</sup>, E.Nakano<sup>b</sup>, O.Nitoh<sup>e</sup>, S.Noguchi<sup>c</sup>, A.Ochi<sup>d</sup>, F.Ochiai<sup>k</sup>, N.Ohishi<sup>b</sup>, Y.Ohnishi<sup>b</sup>, Y.Ohshima<sup>d</sup>, H.Okuno<sup>i</sup>, T.Okusawa<sup>g</sup>, T.Shinohara<sup>e</sup>, A.Sugiyama<sup>b</sup>, S.Suzuki<sup>b</sup>, S.Suzuki<sup>d</sup>, K.Takahashi<sup>e</sup>, T.Takahashi<sup>g</sup>, T.Tanimori<sup>d</sup>, T.Tauchi<sup>a</sup>, Y.Teramoto<sup>g</sup>, N.Toomi<sup>c</sup>, T.Tsukamoto<sup>a</sup>, O.Tsumura<sup>e</sup>, S.Uno<sup>a</sup>, T.Watanabe<sup>d</sup>, Y.Watanabe<sup>d</sup>, A.Yamaguchi<sup>c</sup>, A.Yamamoto<sup>a</sup>, and M.Yamauchi<sup>a</sup>

<sup>a</sup>KEK, National Laboratory for High Energy Physics, Ibaraki-ken 305, Japan

<sup>b</sup>Department of Physics, Nagoya University, Nagoya 464, Japan

<sup>c</sup>Department of Physics, Nara Women's University, Nara 630, Japan

<sup>d</sup>Department of Physics, Tokyo Institute of Technology, Tokyo 152, Japan

<sup>e</sup>Dept. of Appl. Phys., Tokyo Univ. of Agriculture and Technology, Tokyo 184, Japan

<sup>f</sup>Department of Physics, University of Tokyo, Tokyo 113, Japan

<sup>g</sup>Department of Physics, Osaka City University, Osaka 558, Japan

<sup>h</sup>Department of Physics, Purdue University, West Lafayette, IN 47907, USA

<sup>i</sup>Institute for Nuclear Study, University of Tokyo, Tanashi, Tokyo 188, Japan

<sup>j</sup>The Graduate School of Science and Technology, Kobe University, Kobe 657, Japan

<sup>k</sup>Faculty of Liberal Arts, Tezukayama University, Nara 631, Japan

## Abstract

We have carried out inclusive measurements of  $\Lambda(\bar{\Lambda})$  production in two-photon processes at TRISTAN. The mean  $\sqrt{s}$  was 58 GeV and the integrated luminosity was 265 pb<sup>-1</sup>. Inclusive  $\Lambda(\bar{\Lambda})$  samples were obtained under such conditions as no-electron, anti-electron, and remnant-jet tags. The data were compared with theoretical calculations. The measured cross sections are two-times larger than the leading-order theoretical predictions, suggesting the necessity of next-to-leading-order Monte-Carlo generator.

\* submitted for publication.

†Internet address: enomoto@kekvox.kek.jp.

# 1 Introduction

Charm pair production in two-photon processes at  $\sqrt{s}=58$  GeV have been reported in references [1, 2, 3, 4, 5]. All of these papers have reported larger cross sections than that based on the lowest-order (LO) two-photon theory [6, 7], when the Drees-Grassie parametrization [8] in the resolved-photon processes was taken into account. In our previous reports [2, 3, 4] we showed that the charm-pair cross sections approximately agreed with theory when we took into account the next-to-leading-order correction (NLO) to the hard interactions [9], the lower charm-quark mass, and the intrinsic gluon  $P_T$  inside a photon [10], together with the Levy-Abramowicz-Charchula set-1 (LAC1) parametrization [11] for the resolved-photon process. This explanation of excesses, however, must be confirmed by further analysis.

In this article we present an analysis of inclusive  $\Lambda(\bar{\Lambda})$  production in the two-photon reaction using data taken with the TOPAZ detector at TRISTAN. As was demonstrated in our  $K_s$  analysis [3], strange particles enhance the charm fraction in a sample. This analysis is, thus, expected to provide another handle for checking the above-mentioned theoretical arguments. Moreover, since  $\Lambda(\bar{\Lambda})$  is, being a strange baryon, favorably produced from gluon jets [12, 13], we expect to observe the NLO effects directly by measuring the inclusive  $\Lambda(\bar{\Lambda})$  production rates.

In addition, the technique used to tag a remnant-jet using a forward calorimeter [14], which was developed in the  $K_s$  analysis [3], can also be applied in this analysis. We have thus derived inclusive  $\Lambda(\bar{\Lambda})$  cross sections for both direct and resolved-photon processes separately.

## 2 Event selection

The data used in this analysis were obtained with the TOPAZ detector at the TRISTAN  $e^+e^-$  collider, KEK[15, 16]. The mean  $\sqrt{s}$  was 58 GeV and the integrated luminosity was 265 pb $^{-1}$ . A forward calorimeter (FCL), which covered  $0.98 < |\cos \theta| < 0.998$  ( $\theta$  is the polar angle, i.e., the angle with respect to the electron beam), was installed during the course of the experiment. The FCL was made of bismuth germanate crystals (BGO), and was used to anti-tag the beam electrons (positrons) and to tag hadrons (remnant-jets) [14]. The integrated luminosity of the data with the FCL detector was 241 pb $^{-1}$ .

A description of our trigger system can be found in reference [17]. The requirement for the charged-track trigger was two or more tracks with an opening angle greater than 45-90 degrees. The  $P_T$  threshold for charged particles was 0.3-0.7 GeV, which varied depending on the beam conditions.

The event-selection criteria were as follows: there had to be three or more charged particles ( $P_T > 0.15$  GeV,  $|\cos \theta| < 0.77$ ), the invariant mass ( $W_{VIS}$ ) of visible particles ( $|\cos \theta| < 0.77$ ) had to be greater than 2 GeV, the event-vertex position had to be consistent with the interaction point, and the visible energy had to be less than 25 GeV. In total, 280673 events were selected.

## 3 Monte-Carlo simulation

In order to estimate the acceptances and backgrounds in this analysis, we used the following Monte-Carlo simulation programs. Details concerning the event generation of direct as well as resolved-photon and vector meson dominance (VDM) processes can be found in references [1, 2, 18]. Here, we just note the following points. For  $c\bar{c}$  generation, we used the current charm-quark mass of 1.3 GeV to calculate the cross sections for point-like processes and a constituent charm-quark mass of 1.6 GeV for the hadronization procedure, and made a next-to-leading order (NLO) correction by factorization, the details of which can be found in references [1, 2, 9]. Light-quark generation was carried out by using the lowest order (LO) formula with a  $P_T^{min}$  cut of 2.5 GeV. We used the parton density functions by LAC1 [11] for the resolved-photon process, because the experimental data have favored this parametrization [2, 3, 4]. JETSET6.3 [19] was used for hadronization of parton system. Here, we must mention that we used the default values for the baryon production parameters, such as a  $P(qq)/P(q)$  ratio of 0.10 and a

$B\overline{M}\overline{B}$  ratio of 0.5. Generated events were processed through the standard TOPAZ detector simulation program [20], in which hadron showers were simulated with an extended version of GHEISHA 7 [21]. The simulation's handling of hadronic interactions with nuclei has been updated to fit various experimental cross sections.

Using the above-mentioned Monte-Carlo simulations, the trigger efficiency for the sum of the direct and resolved-photon processes was estimated to be 79%, 97% of which represented charged trigger events. The event-selection efficiency after the trigger was obtained to be 80%.

To generate single-photon-exchange hadronic events we used JETSET6.3[19] with the parameter values given in reference [20].

## 4 Tagging conditions

The tagging conditions were as follows. For anti-electron tagging there had to be no energy deposit of more than  $0.4E_b$  in  $|\cos\theta| < 0.998$  (anti-electron tag or anti-tag), where  $E_b$  is the beam energy. The rejected sample was called the electron tag sample. These selected events were from collisions of almost-real photons, for which the equivalent photon approximation was expected to be accurate at the 1% level. When the energy cut was lowered, the number of mistakenly rejected beam remnant hadron (remnant-jets) events became significant, as predicted by Monte-Carlo simulations. This implies the possibility of tagging the resolved-photon process by requiring, for instance,  $500 \text{ MeV} < E_{FCL} < 0.25E_b$ , where  $E_{FCL}$  is the energy deposit in the FCL (remnant-jet tag or rem-tag). The yield of the remnant-jet tag events agreed with our Monte-Carlo simulation within 5% [3]. An event selection without these two tags is hereafter called, a “no-electron tag” or a “no-tag”. Also, data without using the FCL detector were included in this sample. The fractions of anti-electron and remnant-jet tag events to no-tag events were obtained to be 97.6 and 47%, respectively.

In the Monte-Carlo simulations we used the equivalent photon approximation with the photon flux expression [22]

$$f_{\gamma/e}(x_\gamma) = \frac{\alpha_{em}}{2\pi x_\gamma} (1 + (1 - x_\gamma)^2) \ln \frac{P_{max}^2}{P_{min}^2} - \frac{\alpha_{em}}{\pi} \frac{1 - x_\gamma}{x_\gamma},$$

where

$$P_{min}^2 = m_e^2 \frac{x_\gamma^2}{1 - x_\gamma}.$$

We set the  $P_{max}^2$  limit at the smaller of  $P_{T,q}^2 + m_q^2$  and the anti-tag limit  $[2E_b^2(1 - x_\gamma)(1 - \cos\theta_{max})]$ , where  $x_\gamma = 0.4$ ,  $\theta_{max} = 3.2$  degrees], where  $P_{T,q}$  and  $m_q$  are the transverse momentum and the mass of a quark, respectively [23].

The tagging efficiency of the remnant jet for the resolved-photon process was estimated to be  $76 \pm 3\%$ , taking into account an estimate of the FCL noise (described later). We tried to generate remnant partons using two techniques: one was along the beam direction; the other used a Gaussian distribution of the  $P_T$ -width (0.44 GeV) with respect to the beam axis. These two methods differed in acceptance by only 1%. Further, the tagging efficiency of the remnant-jet tag for the direct process was estimated to be  $20 \pm 2\%$  with the estimated level of FCL noise.

## 5 $\Lambda(\overline{\Lambda})$ inclusive analysis

The charged-track selection criteria for the  $\Lambda(\overline{\Lambda})$  analysis were as follows: for each track  $P_T$  had to be greater than 0.15 GeV,  $|\cos\theta|$  had to be less than 0.77, and the closest approach to the interaction point

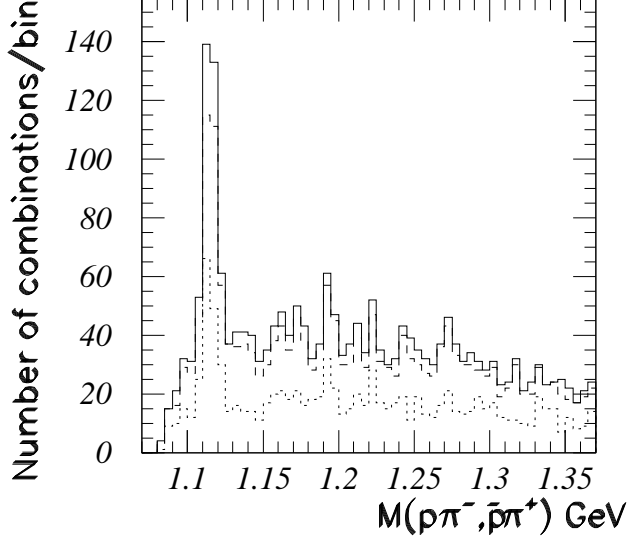


Figure 1: Invariant-mass spectra of  $p\pi^-$ 's and their charge conjugations. The solid histogram is for the no-electron tag, the dashed one is for the anti-electron tag, and the dotted one is for the remnant-jet tag.

in the XY-plane (perpendicular to the beam axis) had to be greater than 0.5 cm. Using these selected tracks, we looked for opposite-sign pairs with an opening angle of less than 90 degrees, and carried out secondary vertex reconstructions three-dimensionally. Here, the  $dE/dx$  of one of two tracks had to be consistent with the proton assumption ( $\chi^2_{p(\bar{p})} < 10$ ), and that of the other had to be consistent with the pion assumption ( $\chi^2_{\pi^\pm} < 10$ ). We demanded that these pairs be consistent with the assumption that they came from event vertices with flight lengths greater than 3 cm. Finally, we rejected pairs which had vertices near ( $\pm 3$ cm) to the inner pressure vessel ( $R_{xy} \sim 30$ cm) or the field cage ( $R_{xy} \sim 33$ cm) of the TPC [16] in order to reduce the background from nuclear interactions; by generating events without any  $\Lambda(\bar{\Lambda})$ 's, we found that there were no significant contribution from such fake pairs after this cut. We also required that  $|\cos\theta|$  of the pair had to be less than 0.77. The invariant-mass distributions of these candidate  $p\pi^-$  pairs and their charge-conjugated states (CC) are plotted in Figure 1 for the three tagging conditions, respectively. These invariant-mass spectra were fitted with the sum of a fifth-order polynomial and a Gaussian distribution, and the peak entries were obtained for no-, anti-, and remnant-jet tags to be  $255 \pm 20$ ,  $215 \pm 19$ , and  $123 \pm 13$   $\Lambda(\bar{\Lambda})$ 's, respectively, in the  $P_T$  range between 0.75 - 2.75 GeV. The peak position and the width were consistent with the detector simulation. Among them,  $2\Lambda\Lambda$ ,  $0\Lambda\bar{\Lambda}$ , and  $0\Lambda\bar{\Lambda}$  pairs were found. In order to derive the differential  $P_T$  cross sections we divided  $P_T$  into four bins, as shown in Table 1.

## 6 Background subtractions

The single-photon-exchange process produced a large background, especially for high- $P_T$   $\Lambda(\bar{\Lambda})$ 's. This background could have been reduced by applying a cut on the total visible energy. However, we avoided this in order to keep the acceptance for high- $P_T$   $\Lambda(\bar{\Lambda})$ 's. Instead, the contamination from the single-photon-exchange process was estimated and subtracted using a Monte-Carlo simulation on a bin-by-bin basis. The background fractions for the no-tag sample were  $3 \pm 1$ ,  $5 \pm 1$ ,  $12 \pm 3$ , and  $16 \pm 3\%$ , respectively, for the  $P_T$  bins shown in Table 1; they were strongly  $P_T$  dependent. We also estimated these fractions for anti- and remnant-jet tags. They were consistent with the above-mentioned values within the statistical errors.

| tag cond.<br>VDM subt. | no-tag<br>-                | anti-tag<br>-  | rem-tag<br>yes | rem-tag<br>no | anti-rem-tag<br>no |
|------------------------|----------------------------|----------------|----------------|---------------|--------------------|
| $P_T$ range<br>(GeV)   | cross sections<br>(pb/GeV) |                |                |               |                    |
| 0.75-1                 | $108 \pm 30$               | $102 \pm 30$   | $29 \pm 11$    | $85 \pm 28$   | $73 \pm 28$        |
| 1-1.25                 | $46 \pm 12$                | $42 \pm 12$    | $17 \pm 6$     | $35 \pm 11$   | $25 \pm 12$        |
| 1.25-1.5               | $13.2 \pm 4.9$             | $12.1 \pm 4.7$ | $5.2 \pm 3.1$  | $7.4 \pm 4.1$ | $6.9 \pm 5.2$      |
| 1.5-2.75               | $5.1 \pm 1.4$              | $3.5 \pm 1.2$  | $2.3 \pm 1.0$  | $2.4 \pm 1.0$ | $1.2 \pm 1.4$      |

Table 1: Differential cross section of  $\Lambda(\bar{\Lambda})$  versus  $P_T$  (GeV) [ $d\sigma/dP_T$  (pb/GeV)], for  $|\cos\theta| < 0.77$ . Six cases are listed: no-tag, anti-electron tag, remnant-jet tag with VDM subtraction, anti-remnant-jet tag without VDM subtraction, and remnant-jet tag without VDM subtraction, which are described in the text.

The background from beam-gas interactions was estimated using the off-vertex events in the beam direction. The beam-gas contribution for a no-tag sample was  $22 \pm 3\%$  on the average, and was subtracted from the data. This was mostly due to a vacuum leak in the beam pipe during some period. It was larger than in the case of the  $K_s$  analysis [3]. For the anti- and remnant-jet tag samples, the above values became  $26 \pm 4$  and  $28 \pm 5\%$ , respectively. Without the anti-tag condition, the beam-gas contribution became slightly larger, suggesting that the electron-tagged events were cleaner.

FCL noise hits were studied by analyzing random-trigger and Bhabha events. The probability of noise hits with  $E_{FCL} > 0.5$  GeV was estimated to be 13.7%, while for hits with  $E_{FCL} > 0.4E_b$  it reduced to be 0.1%. The FCL noise was also related to a vacuum leak. In the Monte-Carlo simulations we added noise hits randomly in accordance with the observed noise-hit probability in order to reliably estimate the tagging efficiencies.

## 7 Systematic errors

The systematic errors for the cross sections were estimated, bin by bin, as follows. For the trigger, we added some extra noise hits in the tracking chambers in the simulations. For the event selection and the  $\Lambda(\bar{\Lambda})$  reconstruction we changed the cut values and evaluated the systematic errors as cross-section differences. We also changed the pulse-height threshold in the TPC simulation in order to evaluate the effects on its tracking efficiency. We added the obtained systematic errors quadratically on a bin-by-bin basis.

In order to investigate the effect of nuclear interactions in the material in front of the TPC, we compared the yields of  $\Lambda$  and  $\bar{\Lambda}$  in the experimental data as well as in the Monte-Carlo data. The ratio  $[N(\Lambda)/N(\bar{\Lambda})]$  was  $1.4 \pm 0.3$  in the experiment, while the Monte-carlo simulation predicted this value to be  $1.43 \pm 0.09$ , being consistent with the data. The deviation from 1.0 was considered to be due to an inelastic scattering of  $\bar{\Lambda}$  with the material in front of the TPC. This occurred mostly in the low- $P_T$  regions. The effect of nuclear interactions was corrected using the Monte-Carlo simulations. The total systematic errors were 16~21%, depending on  $P_T$ , of which the cut dependence in the event selection was the dominant source. These systematic errors were quadratically added to the statistical errors.

We also checked the acceptance ambiguity due to the parametrization dependence of the resolved-photon processes by comparing the LAC1 [11] and Drees-Grassie [DG] [8] parametrizations. The acceptance difference was estimated to be 3.3%, which is small compared to the systematic errors given above.

## 8 Results

The  $P_T$  differential cross sections were obtained from the number of reconstructed  $\Lambda(\bar{\Lambda})$ 's in each bin, and its corresponding efficiency was estimated using the previously described Monte-Carlo simulations. They are listed in Table 1 and plotted in Figures 2 (a) - (d) for the three tagging conditions and two subtraction schemes discussed afterward, respectively. Figure 2 (a) is for anti-electron tag events. In the remnant-jet tag events, the Monte-Carlo simulation predicted a significant contamination from VDM events. The tagging efficiency for the VDM process was estimated to be  $65 \pm 6\%$ , slightly less than that of the resolved-photon process. In addition, there was a large ambiguity in the cross section of the VDM process. We therefore calculated the cross sections using two subtraction schemes. Figure 2 (b) was obtained by subtracting the VDM contribution predicted by the Monte-Carlo simulation (VDM subtraction) for the remnant jet. Here, the “anti-remnant-jet tag” cross section was obtained by subtracting the remnant-jet tag cross section from that of the anti-electron tag. We do not show the cross sections for the anti-remnant-jet tag with VDM subtraction because of low statistics. Figures 2 (c) and (d) were obtained without VDM subtraction. In Figures 2 (b) and (c), the contribution of the direct process was subtracted. The histograms in Figures 2 (a) - (d) are the Monte-Carlo predictions: the cross-hatched, singly-hatched, and open areas are predictions for the direct, resolved-photon (LAC1), and VDM processes, respectively.

## 9 Discussions

The fraction of charm events was studied using the above-mentioned Monte-Carlo simulations. We found that 70% of the events with  $P_T(\Lambda, \bar{\Lambda}) > 1.5$  GeV were of charm origin. On the other hand, only 35% of the events with charged tracks of  $P_T > 1.5$  GeV were from  $c\bar{c}$  pairs. Also, the Monte-Carlo simulations predicted that 55% of these high- $P_T$  charm events originated from the direct process. The contribution of the resolved-photon process is higher than that in the  $K_s$  analysis [3]. This is considered to be due to the existence of gluon jets in the resolved-photon process, even in the LO calculation. In this study we derived six types of cross sections using different tagging conditions and subtraction schemes. We can therefore separately compare each cross section with the theoretical prediction for each process.

Firstly, about 30% of the high- $P_T$  ( $P_T > 1.5$  GeV) events can be explained as electron-tagged events (see Table 1). Secondly, the anti-tag cross section [Figure 2 (a)] is two-times larger than the theoretical model prediction, though the spectrum shape seems to be consistent with it. Here, we must mention that this theoretical model reasonably explained the  $K_s$  inclusive cross section in the previous study [3].

The cross sections with the remnant-jet and anti-remnant-jet tags also show discrepancies having a factor of  $\sim 2$  compared to predictions of the direct, resolved, and VDM processes [Figures 2 (b)-(d)].

The VDM model is considered to be ambiguous, especially in predicting the total cross sections. However, the  $\Lambda(\bar{\Lambda})$ -spectrum of this process is softer than the others and also than the experimental data. We therefore cannot fit it to the experimental data by changing the normalization. Moreover, increasing the normalization factor makes the  $K_s$  cross-section discrepancy in the low- $P_T$  region larger, and inconsistent with the experimental observation [3].

In order to check whether the parton-density functions have anything to do with the discrepancy, we compared our remnant-jet-tag data [Figure 2 (c)] with the predictions from six sets of parametrizations by Hagiwara, Tanaka, Watanabe, and Izubuchi [WHIT1-6] [23]. A systematic analysis on the gluon distributions can be carried out using these parametrizations. We selected those parametrizations which showed higher charm cross sections, i.e., WHIT-1 and -4. The results are shown in Figures 3 (a) and (b), where the histograms are the predictions by the WHIT-1 and -4 parametrizations with  $P_T^{min}$ 's of 2.0 and 2.5 GeV. There are some possible combinations (for example, WHIT-4 with  $P_T^{min} = 2.0$  GeV seems to fit the data better). Notice that these operations do not solve any discrepancies which appeared in the anti-remnant-jet-tag data.

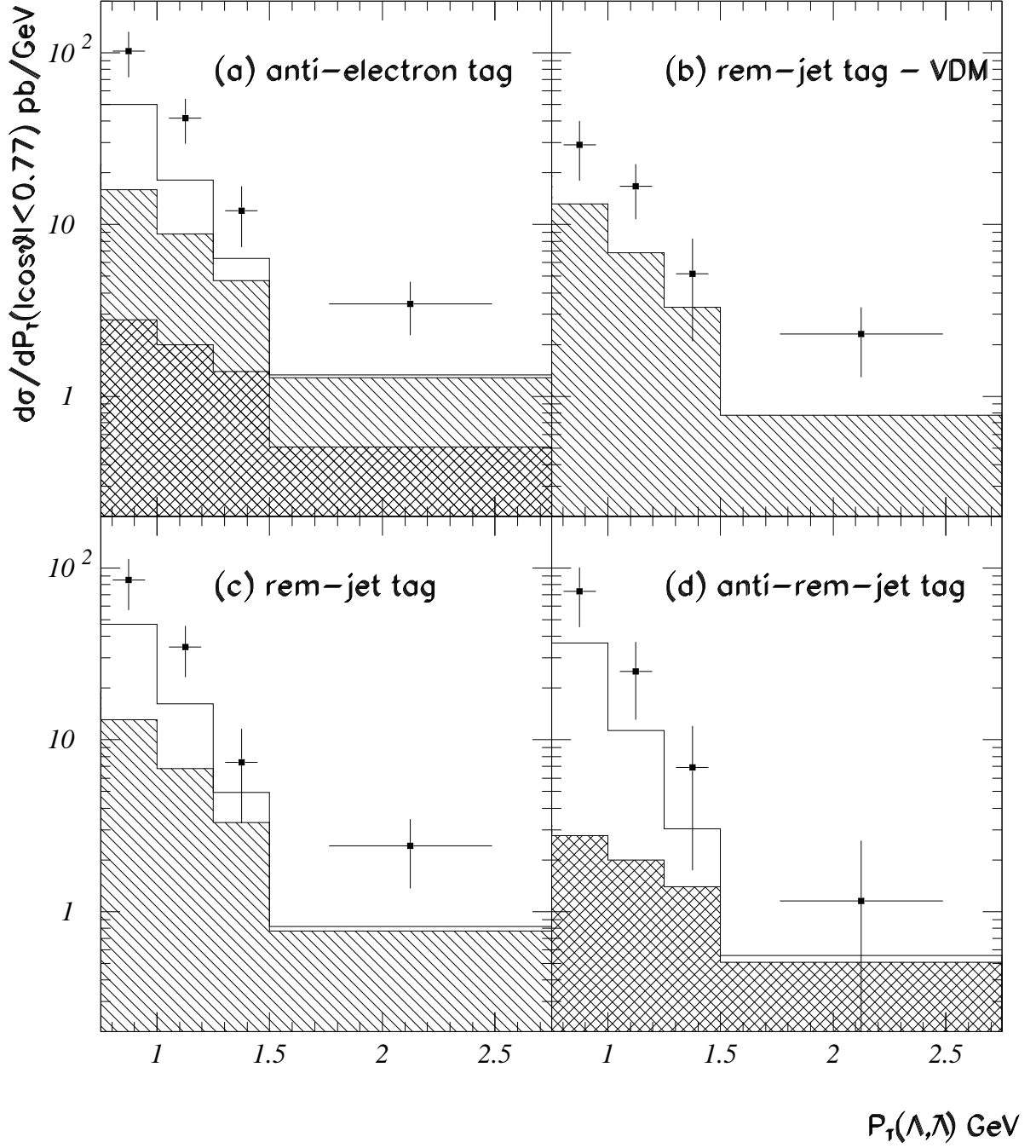


Figure 2: Differential cross section of  $\Lambda(\bar{\Lambda})$  versus  $P_T$  (GeV) [ $d\sigma/dP_T$  (pb/GeV)], for  $|\cos\theta| < 0.77$ . Five cases are plotted: (a) anti-electron tag, (b) remnant-jet tag with the VDM and direct process subtraction, (c) remnant-jet tag without the VDM subtraction, and (d) anti-remnant-jet tag without the VDM subtraction, as described in the text. The corresponding processes are presumably; (b) resolved-photon, (c) resolved-photon and VDM, and (d) VDM and direct processes. The histograms are the theoretical predictions which are described in the text. The open area is for the VDM, the singly-hatched one is for the resolved-photon process, and the cross-hatched one is for the direct process.

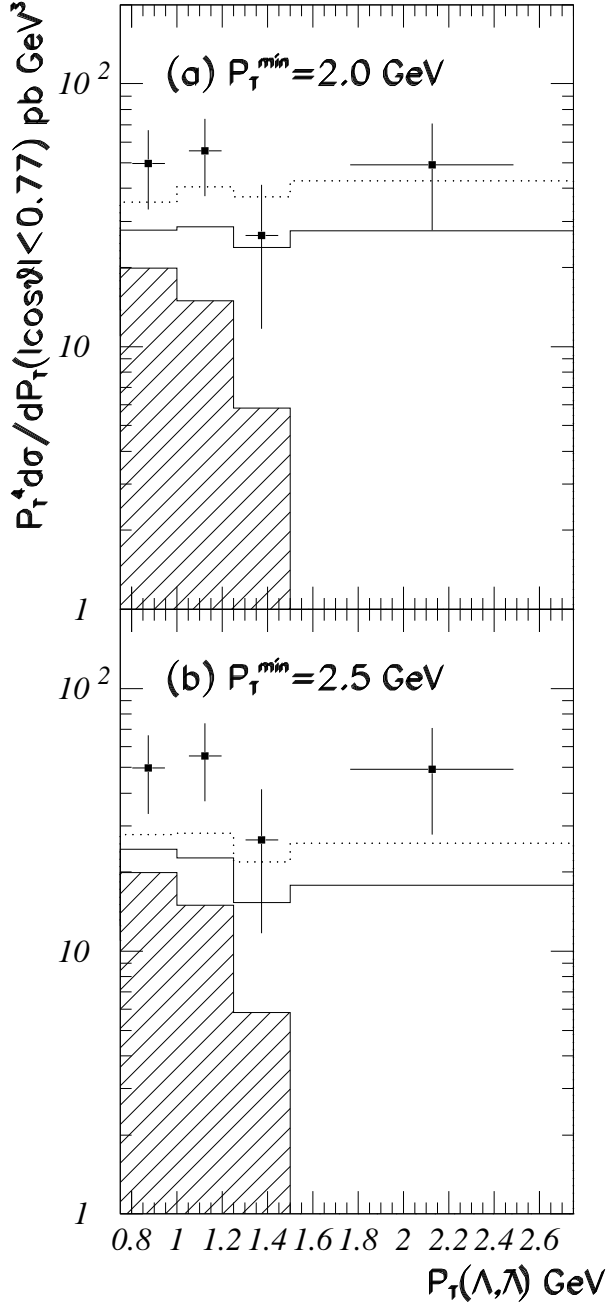


Figure 3: Differential cross section of  $\Lambda(\bar{\Lambda})$  versus  $P_T$  (GeV) [ $P_T^4 d\sigma / dP_T$  (pb·GeV<sup>3</sup>)], for  $|\cos\theta| < 0.77$  for the remnant-jet tag without the VDM subtraction. The hatched areas are the predictions by the VDM Monte-Carlo simulation. The histograms are predictions by the WHIT-1 and -4 parametrizations. The solid one is WHIT 1 and the dotted one WHIT-4. Two values of  $P_T^{\min}$ 's were used, i.e., (a) 2.0 and (b) 2.5 GeV.

| tag cond.      | Experiment | Theory (LO) | Exp./Theory | subprocess          |
|----------------|------------|-------------|-------------|---------------------|
| antitag        | 43.3±8.3   | 19.1        | 2.26±0.43   | VDM+resolved+direct |
| rem-tag (-VDM) | 15.6±3.5   | 6.0         | 2.60±0.58   | resolved            |
| rem-tag        | 34.8±7.8   | 17.3        | 2.01±0.45   | VDM+resolved        |
| anti-rem       | 27.7±7.9   | 13.1        | 2.11±0.60   | VDM+direct          |

Table 2: Total cross section (pb) of  $\Lambda(\bar{\Lambda})$  in the  $|\cos\theta| < 0.77$  and  $0.75 < P_T < 2.75$  GeV range. The notation (-VDM) means the VDM subtraction which was described in the text. Here, we use the LO theories in order to show the discrepancy with the experimental data.

In order to reduce these discrepancies we may need an NLO correction to the light-quark events, which is absent from our present Monte-Carlo generator.

Our Monte-Carlo generation of  $\gamma\gamma$  events was based on the LO matrix element calculations in the hard processes. Although the total cross section of the direct process was increased by a factor of 1.31 [9, 2, 3, 4], and the  $P_T$  ( $P_T$  of parton)-dependent factor was used in the resolved-photon processes [2, 3, 4], our Monte-Carlo generator has no explicit hard gluon emissions, which should exist in a truly NLO generator. We consider that the discrepancies between the data and the theory can be attributed to these effects, based on the baryon abundance in the experimentally observed gluon jets [12, 13]. The baryon excess in the gluon jets has not yet been established in a sufficiently quantitative way. When it is, our data will be direct evidence of the NLO effect.

We show in Table 2 the total cross sections of  $\Lambda(\bar{\Lambda})$  in the  $|\cos\theta| < 0.77$  and  $0.75 < P_T < 2.75$  GeV range. In order to extract the NLO effect, we calculated the LO cross sections, which are also shown in Table 2. Here, we removed the NLO factorization from our Monte-Carlo generator. The ratio between the theoretical predictions and the experimental data are typically  $\sim 2$ .

## 10 Conclusion

We carried out an inclusive measurement of  $\Lambda(\bar{\Lambda})$  productions in two-photon processes at TRISTAN. The mean  $\sqrt{s}$  was 58 GeV and the integrated luminosity was  $265 \text{ pb}^{-1}$ . Inclusive  $\Lambda(\bar{\Lambda})$  cross sections in two-photon processes were obtained under such conditions as no-electron, anti-electron, and remnant-jet tags. In particular, using the remnant-jet tagging we could unambiguously extract the contribution from the resolved-photon process. Comparisons with theoretical predictions were carried out. The cross sections were two-times larger than the theoretical predictions without hard gluon emissions, suggesting the necessity of next-to-leading-order Monte-Carlo generator.

## Acknowledgement

We thank Drs. K. Hagiwara and T. Sjöstrand for helpful discussion concerning the baryon production mechanism. We also thank the TRISTAN accelerator staff for the successful operation of TRISTAN. The authors appreciate all of the engineers and technicians at KEK as well as those of the collaborating institutions: H. Inoue, N. Kimura, K. Shiino, M. Tanaka, K. Tsukada, N. Ujiie, and H. Yamaoka.

## References

- [1] R. Enomoto et al., Phys. Rev. **D50**, 1879 (1994).
- [2] R. Enomoto et al., Phys. Lett. **B328**, 535 (1994).

- [3] R. Enomoto et al., KEK Preprint 94-106, to be published in Phys. Lett. **B**.
- [4] M. Iwasaki et al., KEK Preprint 94-109, to be published in Phys. Lett. **B**.
- [5] S. Uehara et al., Z. Phys. **C 63** (1994) 213.
- [6] See e.g. S. J. Brodsky, T. Kinoshita, and H. Terazawa, Phys. Rev. **D4** (1971) 1532.
- [7] S. J. Brodsky, T. A. DeGrand, J. F. Gunion, and J. H. Weis, Phys. Rev. Lett. **41** (1978) 672; Phys. Rev. **D19** (1979) 1418; H. Terazawa, J. Phys. Soc. Japan, **47** (1979) 355; K. Kajantie and R. Raitio, Nucl. Phys. **B159** (1979) 528.
- [8] M. Drees and K. Grassie [DG], Z. Phys. **C28** (1985) 451.
- [9] M. Drees, M. Krämer, J. Zunft, and P. M. Zerwas, Phys. Lett. **B306** (1993) 371.
- [10] T. Sjöstrand, CERN-TH.6488/92.
- [11] H. Abramowicz, K. Charchula, and A. Levy [LAC], Phys. Lett. **B269** (1991) 458.
- [12] H. Aihara et al., Phys. Rev. Lett. **53** (1984) 130.
- [13] B. Andersson, G. Gustafson, T. Sjöstrand, Physica. Scripta. **Vol. 32** (1985) 574.
- [14] H. Hayashii et al., Nucl. Instrum. Method., **A316** 202 (1992).
- [15] A. Imanishi et al., Nucl. Instrum. Methods, **A269** 513 (1988); A. Yamamoto et al., Jpn. J. Appl. Phys. Lett., **25** L440 (1986); S. Kawabata et al., Nucl. Instrum. Methods, **A270** 11 (1988); J. Fujimoto et al., Nucl. Instrum. Methods, **A256** 449 (1987); S. Noguchi et al., Nucl. Instrum. Methods, **A271** 464 (1988).
- [16] T. Kamae et al., Nucl. Instrum. Methods, **A252** 423 (1986).
- [17] R. Enomoto et al., Nucl. Instrum. Methods, **A269** 507 (1988); R. Enomoto, K. Tsukada, N. Ujiie, and A. Shirahashi, IEEE Trans. NS. **Vol. 35, No. 1**, 419 (1988); T. Tsukamoto, M. Yamauchi, and R. Enomoto, Nucl. Instrum. Meth. **A297** 148 (1990).
- [18] H. Hayashii et al., Phys. Lett. **B314** (1993) 149.
- [19] T. Sjöstrand, Comput. Phys. Commun., **39** (1986) 347; T. Sjöstrand and M. Bengtsson, Comput. Phys. Commun., **43** (1987) 367.
- [20] I. Adachi et al., Phys. Lett. **B227** (1989) 495.
- [21] H. Fesefeldt, Nucl. Instrum. Meth. **A 267** (1988) 367.
- [22] S. Frixione, M. L. Mangano, P. Nason, and G. Ridolfi, Phys. Lett. **B 319**, 339 (1993).
- [23] H. Hagiwara, M. Tanaka, I. Watanabe, and T. Izubuchi [WHIT], KEK Preprint 93-160, submitted for publication.